

# Chemotaxis of MDCK-F cells toward fibroblast growth factor-2 depends on transient receptor potential canonical channel 1

Anke Fabian · Thomas Fortmann · Etmar Bulk ·  
Valerie C. Bomben · Harald Sontheimer ·  
Albrecht Schwab

Received: 23 August 2010 / Revised: 2 November 2010 / Accepted: 3 November 2010 / Published online: 1 December 2010  
© Springer-Verlag 2010

**Abstract** Movement toward the source of a chemoattractant gradient is a basic cellular property in health and disease. Enhanced migration during metastasis involves deregulated growth factor signaling. Growth factor stimulation and cell migration converge both on the important second messenger  $\text{Ca}^{2+}$ . To date, the molecular identification of  $\text{Ca}^{2+}$  entry pathways activated by growth factors during chemotaxis is still an open issue. We investigated the involvement of the nonselective  $\text{Ca}^{2+}$  channel TRPC1 (transient receptor potential canonical 1) in FGF-2 guided chemotaxis by means of time-lapse video microscopy and by functional  $\text{Ca}^{2+}$  measurements. To specifically address TRPC1 function in transformed MDCK cells we altered the expression levels by siRNA or overexpression. We report that TRPC1 channels are required for the orientation of transformed MDCK cells in FGF-2 gradients because TRPC1 knockdown or pharmacological blockade prevented chemotaxis. Stimulation with FGF-2 triggered an immediate

$\text{Ca}^{2+}$  influx via TRPC1 channels that depended on phospholipase C and phosphatidylinositol 3-kinase signaling. Impeding this  $\text{Ca}^{2+}$  influx abolished chemotaxis toward FGF-2. This functional connection correlated with clustering of FGF receptors and TRPC1 channels as was observed by immunolabeling. These findings show the important interplay between growth factor signaling and  $\text{Ca}^{2+}$  influx in chemotaxis.

**Keywords** Chemotaxis · Calcium · TRPC1

## Introduction

Para- or autocrine growth factor stimulation is an important determinant of tumor progression and aggressiveness and involves  $\text{Ca}^{2+}$  as a second messenger. Fibroblast growth factor-2 is one of the major signal molecules involved in such feedback systems leading to enhanced proliferation, angiogenesis and increased motility and invasion of carcinomas [15, 22]. Interference with abnormal FGF-2 signaling is therefore a means to prevent the formation of metastases. Activation of FGF receptor-1 (FGFR-1) by FGF-2 is enhanced by cell surface heparin sulfate proteoglycans (HSPG) and activates multiple intracellular pathways such as phospholipid or mitogen-activated protein (MAP) kinase signaling. Finally, FGF-2 can trigger a dose-dependent elevation of  $[\text{Ca}^{2+}]_i$ , which is mediated by transient receptor potential canonical-1 (TRPC1) channels in endothelial cells [3, 31]. In MDCK cells, heterologous expression of FGFR-1 results in loss of epithelial properties and gain of a fibroblast-like morphology like during transformation to carcinoma cells [30]. Here, we studied FGF-2 induced  $\text{Ca}^{2+}$  signals in MDCK-F cells that were

Anke Fabian and Thomas Fortmann contributed equally to this work.

**Electronic supplementary material** The online version of this article (doi:10.1007/s00424-010-0901-6) contains supplementary material, which is available to authorized users.

A. Fabian (✉) · T. Fortmann · E. Bulk · A. Schwab (✉)  
Institute of Physiology II, University of Münster,  
Robert-Koch-Str. 27b,  
48149, Münster, Germany  
e-mail: afabian@uni-muenster.de

A. Schwab  
e-mail: aschwab@uni-muenster.de

V. C. Bomben · H. Sontheimer  
Department of Neurobiology,  
Center for Glial Biology in Medicine, University of Alabama,  
Birmingham, AL 35294, USA

transformed by sustained alkaline stress [32]. Migration of MDCK-F cells can be stimulated with FGF-2 as they express the FGFR-1 [19]. Moreover, MDCK-F cells are an established model for studying the role of ion transport proteins in cell migration [36].

Serving as  $\text{Ca}^{2+}$  entry pathways, TRP channels are key regulators of the intracellular concentration of free calcium ( $[\text{Ca}^{2+}]_i$ ). The pathophysiological importance of TRP channels arises from the fact that  $\text{Ca}^{2+}$  is a crucial signaling molecule for every cell type and deregulation of  $[\text{Ca}^{2+}]_i$  can be the cause of several diseases [1]. TRPC channels are expressed in a variety of different cells including MDCK cells [5, 7]. TRPC channels are mainly activated by phospholipase C (PLC) mediated pathways [40] downstream of G-protein coupled receptors or receptor tyrosine kinases. PLC hydrolyzes phosphatidyl-4,5-bisphosphate ( $\text{PIP}_2$ ) into inositol 1,4,5-triphosphate ( $\text{IP}_3$ ) and diacylglycerol (DAG).  $\text{IP}_3$  mainly opens intracellular  $\text{Ca}^{2+}$  stores and DAG can physiologically activate TRPC3/6/7 whereas TRPC1/4/5 channels alone seem to be unresponsive to DAG [18, 24]. But DAG can also influence TRPC1 indirectly via heteromerization with TRPC3 [9, 25, 26] or via activation of protein kinase C (PKC). PKC can phosphorylate TRPC1 [2], whereby it activates TRPC channel heteromers including TRPC1 and TRPC5 [34].

Another phospholipid cascade that leads to TRPC1 activation implies production of phosphatidylinositol 3,4,5-trisphosphate ( $\text{PIP}_3$ ) by phosphatidylinositol 3-kinase (PI3K) as shown in vascular myocytes [33]. As it is becoming clear that TRPC1 channels are activated following receptor stimulation via PLC and PI3K, we investigated whether FGF-2 also acts via these pathways.

In the pathophysiological context of metastatic cancer disease, migration of epithelial cancer cells away from the primary tumor toward blood or lymphatic vessels comprises a critical step in the metastatic cascade. On the cellular level cell migration is orchestrated among others by the fine-tuned  $[\text{Ca}^{2+}]_i$  [8, 11, 21, 45].  $\text{Ca}^{2+}$  conveys polarity to migrating cells and coordinates processes such as actin dynamics or reorganization of focal adhesions [4, 46]. Stretch-activated  $\text{Ca}^{2+}$  channels of unknown molecular identity have been implicated in the regulation of adhesion and force generation of randomly migrating keratocytes [10, 23]. The molecular identity of  $\text{Ca}^{2+}$  channels regulating cell migration is still unclear. However, recent studies indicate that TRP channels are involved in cell migration and related processes [27, 43]. Stretch-activated or chemoattractant stimulated  $\text{Ca}^{2+}$  entry via TRPM7 channels leads to the formation of dynamic microdomains of high  $[\text{Ca}^{2+}]_i$  in the leading lamella of embryonic lung fibroblasts [44]. Moreover, migrating MDCK-F cells form a narrow  $\text{Ca}^{2+}$  gradient at the front that is lost after TRPC1 silencing leading to loss of

intrinsic cell directionality [13]. And finally, neuronal path finding via external chemotropic guidance depends on  $\text{Ca}^{2+}$  entry via TRPC1 channels [38, 42].

Although it is becoming clear that  $\text{Ca}^{2+}$  is a key second messenger in growth factor signaling of tumors and also in chemotaxis, the molecular connection is still largely unknown. In the present study, we investigated the processes that facilitate chemotaxis of MDCK-F cells toward FGF-2: growth factor induced lipid signaling (PLC, PI3K) and  $\text{Ca}^{2+}$  entry via TRPC1 channels.

## Methods

### Cell culture

Alkaline-transformed Madin–Darby canine kidney (MDCK-F) cells were cultivated in bicarbonate-buffered Minimal Essential Medium (MEM; pH 7.4) with Earle's salts (PAA Laboratories, Pasching, Austria) containing 10% fetal calf serum (Biochrom, Berlin, Germany) in a 37°C humidified atmosphere of 5%  $\text{CO}_2$ . The experiments were mainly carried out with two different cell lines: one cell line with a stably enhanced expression of the human N-terminally HA-tagged TRPC1 isoform (hTRPC1-HA), one with a stably reduced TRPC1 expression via short interfering RNA (siTRPC1) using the pSuper.retro.puro vector as described [13]. For control experiments, we established a vector control cell line that was transfected with the empty expression vector (pcDNA3) and a siMock control cell line that was generated by transfecting MDCK-F cells with the pSuper.retro.puro vector carrying a mock oligo. The migratory behavior of the two control cell lines was indistinguishable and corresponds to that of wt MDCK-F cells [13].

### Chemotaxis experiments

Migration of MDCK-F cells was captured by means of time lapse video microscopy as already described [13]. One day prior to the experiments the cells were seeded in fibronectin ( $1.4 \mu\text{g}/\text{cm}^2$ ) coated ibidi- $\mu$ -slides (Ibidi, Munich, Germany). The  $\mu$ -slides were put into heated chambers (37°C) mounted on inverted microscopes (Axiovert25, Carl Zeiss, Inc., Gottingen, Germany) and the cells were equilibrated to serum-free MEM with Earle's salts for 1 h. Also, blockers were usually applied 1 h before the start of the recordings. Chemotaxis experiments were performed in a paired fashion. We observed the cells 1 h without chemoattractant stimulation, before we established a gradient of FGF-2: A  $\mu$ -slide consists of two reservoirs connected via a 100- $\mu\text{l}$  channel. By filling one reservoir with medium and the other with medium containing FGF-2 (10,000 $\times$  concentrated) and

Patentblue V (Sigma) and tilting the chamber for a second we could establish a sharp gradient as visualized by coapplication of Patentblue V. At the center of observation the FGF-2 concentration amounted to a value of 5 ng/ml. Subsequently, chemotaxis was monitored for 3 h. The acquisition interval was 5 min throughout the entire experiment. Images were acquired with video cameras (Models XC-ST70CE and XC-77CE, Hamamatsu/Sony, Japan) and PC-vision frame grabber boards (Hamamatsu, Herrsching, Germany), controlled by HiPic and WASABI software (Hamamatsu). The outlines of the cells were marked at each time step throughout the entire image stack applying the AMIRA software (TGS, San Diego, CA). The cell contours then served as the basis for further analysis. Parameters such as migratory velocity ( $\mu\text{mmin}^{-1}$ ) and translocation ( $\mu\text{m}$ ) were analyzed using self-made JAVA programs and the NIH ImageJ software (<http://rsb.info.nih.gov/ij/>). Migration was determined as the movement of the cell center per time unit. In order to determine the directionality of migration with respect to the FGF-2 gradient we determined the mean movement of the cell centers in parallel to the FGF-2 gradient as a function of time. This corresponds to the movement in  $x$ -direction of a coordinate system.

#### Western blot

MDCK-F cells were seeded in 6- or 10-cm culture dishes. The cells were washed with ice-cold phosphate-buffered saline (PBS) three times and lysed with RIPA buffer containing: 25 mM Tris-HCl, 150 mM NaCl, 1% Nonidet P40, 0.1% SDS, 1% Sodium Deoxycholate; phosphatase inhibitor (PhosSTOP; Roche) and protease inhibitor (cOmplete, Mini; Roche) cocktail tablets were added following the manufacturer's information. When probing ERK phosphorylation cells kept serum-free for at least 12 h. They were lysed either directly (control) or they underwent a treatment as indicated. After lysis, insoluble material was removed by centrifugation for 5 min at  $12,846\times g$  at  $4^\circ\text{C}$ . Protein quantification of the lysates allowed loading of equal protein amounts for SDS-PAGE (7.5%) before transfer to nitrocellulose membranes (PROTRAN, Schleicher Schuell, Dassel, Germany). After blotting, unspecific binding sites were blocked with Western Blot solution (5% fat free milk, 0.5% Tween in PBS) for 1 h and the membranes were incubated with the primary antibody (monoclonal mouse anti-phospho-ERK1/2 (p44/42 MAPK) (Thr 202/204) (E10; Cell Signalling Technology), 1:1,000 or anti TRPC3 antibody, 1:200 (Alomone)—in the same solution at  $4^\circ\text{C}$  overnight. The next day, the membrane was washed  $3\times 10$  min with PBS/0.5% Tween and incubated with a peroxidase-conjugated secondary antibody—goat anti-mouse IgG or anti-rabbit (Dianova; 1:50,000 or

1:10,000, respectively). After 1 h, the blot was washed three times with PBS/0.5% Tween and developed using an enhanced chemiluminescence detection reagent kit (Thermo Scientific Rockford, Rockford, IL). To ensure equal loading the blot was stripped and stained with a monoclonal antibody against  $\beta$ -actin-mouse anti- $\beta$ -actin (Clone AC-15, #A5441, Sigma) 1:10,000. Here, we used the same secondary antibody as already mentioned. The experiments were repeated three to four times. Western blots were quantified by means of densitometry.

#### Intracellular $\text{Ca}^{2+}$ measurements

One to two day(s) prior to the experiment cells were seeded on fibronectin ( $1 \mu\text{g}/\text{cm}^2$ ) coated glass bottom dishes (Willco wells, Amsterdam, The Netherlands). The cells were preincubated with Ringer solution (in mM: NaCl 122.5, KCl 5.4,  $\text{CaCl}_2$  1.2,  $\text{MgCl}_2$  0.8, D-glucose 5.5, HEPES 10.0, pH 7.4) and fura-2-AM (3  $\mu\text{M}$ ; Calbiochem) for dye loading at RT for 25 min. The experiments were carried out at  $37^\circ\text{C}$ , and cells were continuously superfused with Ringer solution. Excitation wavelength alternated between 340 and 380 nm. The emitted fluorescence was monitored at 500 nm. CoolSnap camera, monochromator and data acquisition were controlled by Metafluor Software (Visitron Systems). Fluorescence intensities were corrected by background subtraction and measured in 20-s intervals over the entire cell area.  $[\text{Ca}^{2+}]_i$  was calculated as described before [11]. Briefly,  $\text{Ca}^{2+}$  measurements were calibrated at the end of each experiment. Maximal and minimal ratios were determined separately for each cell by the application of ionomycin-containing (1  $\mu\text{M}$ ) Ringer solutions containing either 5 mM EGTA or 5 mM  $\text{Ca}^{2+}$ . For each cell clone at least 45 cells were analyzed and mean values and S.E.M. of the calculated  $[\text{Ca}^{2+}]_i$  over a 10-min period are presented. Significance was tested with the Student's *t* test.

We applied the manganese ( $\text{Mn}^{2+}$ ) quenching assay to obtain an indirect measure of FGF-2 induced  $\text{Ca}^{2+}$  influx via  $\text{Ca}^{2+}$  channels.  $\text{Mn}^{2+}$  can enter the cell via  $\text{Ca}^{2+}$  channels, bind to fura-2 with higher affinity than  $\text{Ca}^{2+}$  and decrease fluorescence intensity of the former [29]. Thus, the decrease in fluorescence intensity can be taken as an indirect measure of  $\text{Ca}^{2+}$  influx. To this end cells were excited at the isosbestic wavelength of fura-2 at 365 nm. Using this wavelength, the emitted fluorescence at 500 nm is independent of the  $[\text{Ca}^{2+}]_i$  and the decay of fluorescence intensity can be ascribed to  $\text{Mn}^{2+}$  quenching. The fluorescence intensity was monitored in 3-s intervals. Experiments were performed in a paired fashion: following an initial equilibration period control Ringer solution was replaced by a modified Ringer solution containing 50  $\mu\text{M}$   $\text{MnCl}_2$ . After 2 min this solution was exchanged for one containing 50  $\mu\text{M}$   $\text{MnCl}_2$ , 10 ng/ml fibroblast growth factor-2

(Peprotech GmbH, Hamburg, Germany) and blockers as indicated. For each cell clone and condition at least 28 cells ( $N \geq 3$  individual experiments) were analyzed and mean fura-2 fluorescence quenching (% of fluorescence intensity  $F_{365}$  at  $t=0$ )  $\pm$  SEM is shown. Regression analysis of fluorescence intensities over time was performed to determine the change in quenching rates QR ( $F_{365}$ ) [%/s] before and after the stimulus. Experiments were performed for at least three times and significance was tested with the Student's *t* test.

### Immunofluorescence

After plating on poly-L-lysine coated cover slips cells were serum-starved for at least 12 h. Subsequently, the cells were fixed with 4% paraformaldehyde in PBS at room temperature for 20 min. Triton X-100 (0.1%) in 4% paraformaldehyde in PBS was applied for 1 min to increase permeabilization. After washing with PBS non-specific binding sites were blocked with 10% (v/v) goat normal serum (Sigma, Germany) in 10 mM  $\text{Na}_2\text{HPO}_4$  and 150 mM NaCl for 30 min. Cells were double-stained for 1 h with monoclonal antibodies against the FGF receptor-1 (1:100; QED Biosciences Inc., USA) and monoclonal rat anti-HA recognizing the HA tag of transfected TRPC1 channels (1:200 clone 3 F10; Roche, Germany). After washing the following secondary antibodies were applied for 1 h: Alexa568-conjugated anti-mouse IgG (1:500 Invitrogen/Molecular Probes, USA) and Alexa-488 conjugated goat anti-rat IgG (1:400 Invitrogen/Molecular Probes, USA). The cover slips were covered with Dako fluorescence mounting medium (Dako GmbH, Germany). We performed the following staining controls to ensure specificity: stainings of nontransfected cells, stainings using only the secondary antibody, double stainings against TRPC1 or FGFR-1 and another target protein that did not colocalize. We used the following filters for detection: Alexa-488, D470/40 nm excitation, 515–565 nm emission; Alexa-568, D540/25 nm excitation, D605/55 nm emission. Images were taken using an inverted microscope (Axiovert S100, Carl Zeiss, Germany) with a  $100\times$  1.45 oil immersion objective and a back-illuminated EM-CCD camera Andor DU888 (Andor) controlled by MetaMorph software.

To quantify the level of colocalization pixels with highest fluorescence intensity were assigned as optical centers. Dual-color images were superimposed, the pixel-shift was corrected and the number and distances of optical centers were determined. Intensity spots were counted in areas of  $5,000 \text{ pixel}^2$  in every cell. At least  $n=30$  cells from three independent stainings were analyzed. Data are presented as means  $\pm$  SEM. Significance was tested with Student's *t* test.

## Results

### Chemotaxis toward FGF-2 requires TRPC1 channels

To analyze the effects of FGF-2 stimulation on TRPC1 channels during chemotaxis we compared MDCK-F cells whose TRPC1 expression levels were altered either by stable expression of siRNA against TRPC1 (siTRPC1) or by overexpression of a human HA-tagged TRPC1 isoform (hTRPC1-HA). The expression level of the siTRPC1 cell line was reduced to 30% whereas the hTRPC1-HA cell clone gained a doubled expression compared to respective controls (vector and siMock) as already shown [13]. These two opposing cell lines enabled us to get insights into the role of TRPC1 during externally guided cell migration because we could not detect a compensatory upregulation of other TRPC channels. TRPC3 and TRPC6 channels were expressed at the same level in all cell lines as assessed by Western blot analysis and RT-PCR (see Fig. S1). We also compared siTRPC1 cells and TRPC1 overexpressing cells with the respective control cell lines whose TRPC1 expression level was not modified. The migratory behavior of these two control cell lines carrying two different vectors is identical and corresponds to that of wt MDCK-F cells [13].

We had previously demonstrated that siTRPC1 cells migrate more slowly and less efficiently than hTRPC1-HA cells. Migration speed and translocation of siTRPC1 cells were approximately 20% and 30% lower, respectively, than those of hTRPC1-HA cells [13]. Compared to (vector and siMock) control cells the mean squared displacement of randomly moving hTRPC1-HA overexpressing cells was significantly higher. In accordance with this study we detected again random movement of these cells in the absence of an FGF-2 gradient. We now established a stable FGF-2 gradient and the same cells were subsequently challenged for their ability to chemotax along this gradient for 3 h. In the center of observation the FGF-2 concentration amounted to an estimated value of 5 ng/ml. The speed of neither hTRPC1-HA overexpressing cells, siTRPC1 or control cells were affected by the presence of the FGF-2 gradient. However, hTRPC1-HA overexpressing cells clearly reoriented and chemotaxed toward FGF-2 as displayed by net *x*-translocation up the FGF-2 gradient (Fig. 1a and c). Thus, after 175 min hTRPC1-HA cells reached a mean *x*-translocation of  $20.3 \pm 8.5 \mu\text{m}$  ( $n=35$ ) toward the source of FGF-2. In contrast and as shown in Fig. 1b and d, siTRPC1 cells did not chemotax toward FGF-2 gradients as revealed by mean *x*-translocations alternating around zero from the beginning until the end of the experiment ( $-5.4 \pm 6.8 \mu\text{m}$ ;  $n=35$ ). Also, vector and siMock control cells clearly chemotaxed toward FGF-2 reaching a net *x*-translocation of  $29 \pm 7.7 \mu\text{m}$  ( $n=27$ ;



**Fig. 1** Chemotaxis in FGF-2 gradients depends on TRPC1 expression and function. Cells with increased and reduced TRPC1 expression (plus respective controls) were recorded by time-lapse video microscopy while migrating in FGF-2 gradients with increasing concentrations from left to right. **a** During 3 h after gradient formation, hTRPC1-HA overexpressing cells translocated into the direction of the FGF-2 gradient as indicated by the superimposed outlines of the cells at their start and end positions. **Arrows** mark the trajectories from start (white dot) to end of observation (arrowhead). **b** In contrast, siTRPC1 cells did not respond to FGF-2 as indicated by the superimposed outline of the cells at their start positions and their trajectories pointing toward lower FGF-2 concentrations. **c** Chemotaxis was quantified by plotting the movement of the cells into the direction of the FGF-2 gradient ( $x$ -direction). Mean  $x$ -translocations  $\pm$  SEM are presented as a function of time. Positive mean  $x$ -translocation of hTRPC1-HA overexpressing cells represents movement toward higher FGF-2 concentrations, i.e., their ability to chemotax toward FGF-2. Chemotaxis was abolished by 10  $\mu$ M GsMTx-4. **d** Silencing of TRPC1 in siTRPC1 cells abrogated chemotaxis toward FGF-2. **e, f** Also siMock and (empty) vector control cells showed chemotaxis

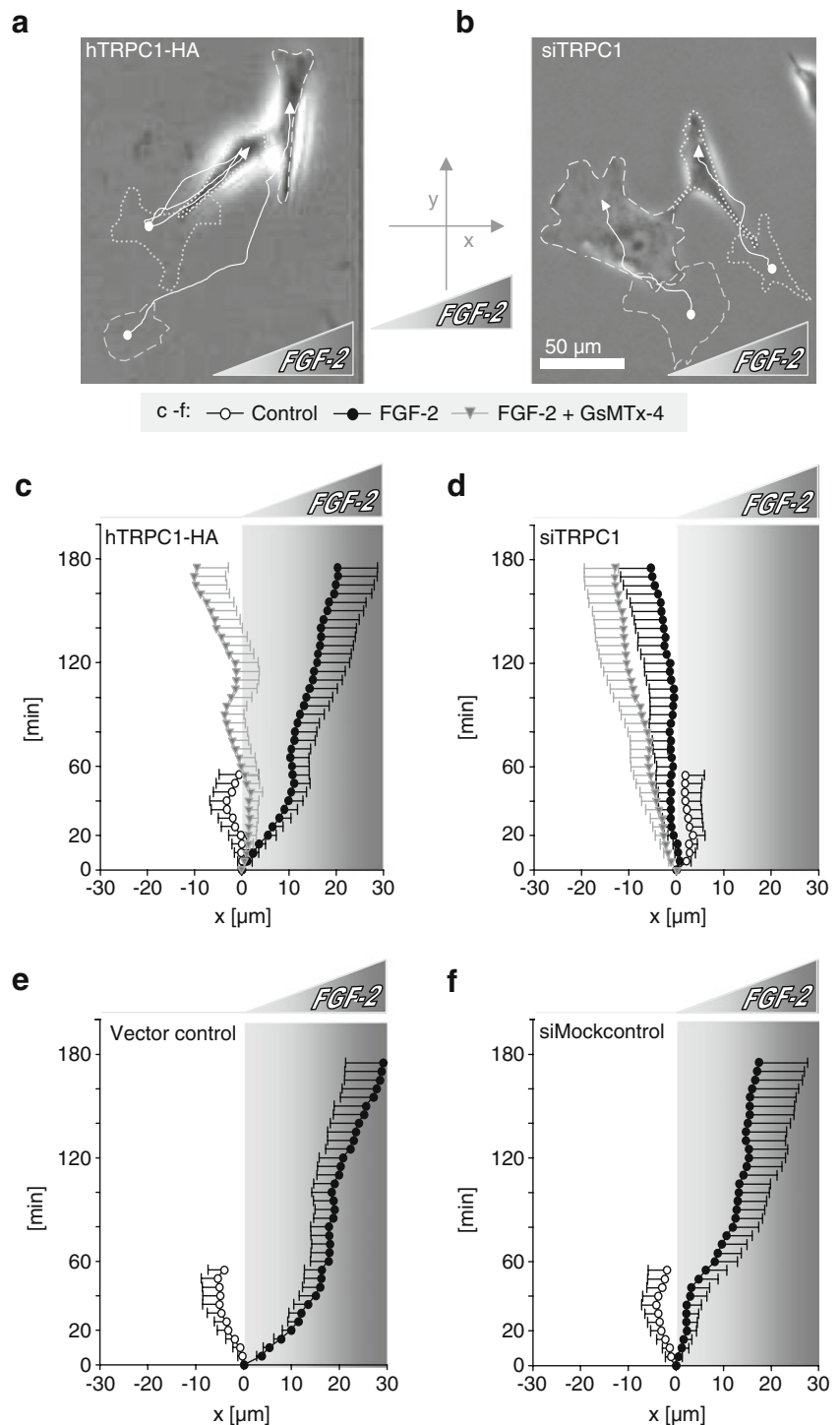
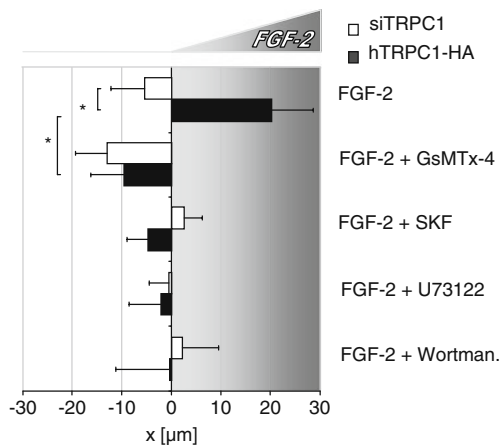


Fig. 1e) and  $17.7 \pm 9.9 \mu\text{m}$  ( $n=27$ ; Fig. 1f), respectively. Thus, TRPC1 expression levels correlated positively with the cells' ability to sense and move toward the source of a chemical gradient of FGF-2. Accordingly, hTRPC1-HA cells no longer chemotaxed toward FGF-2 when incubated with the TRP channel inhibitor GsMTx-4 (10  $\mu$ M)—an inhibitor of stretch-activated channels [6] or SKF96365 (25  $\mu$ M)—a nonselective inhibitor of L-type and receptor-

operated  $\text{Ca}^{2+}$  channels (see summary of the chemotaxis experiments in Fig. 2). In the presence of each of these blockers, both cell lines behaved identically.

We next investigated the FGF-2 triggered signaling cascades that might activate TRPC1 channels. To this end, we performed chemotaxis experiments in the presence of PLC and PI3K blockers U73122 (50 nM) and Wortmannin (50 nM), respectively. As shown in Fig. 2 inhibition of both



**Fig. 2** Chemotaxis toward FGF-2 depends on TRPC1 and lipid signaling. Summary of chemotaxis experiments as indicated by the net mean  $x$ -translocation  $\pm$  SEM at the end of the experiment (175 min). Positive mean  $x$ -translocation indicates chemotaxis. Silencing of TRPC1 (siTRPC1) or pharmacological inhibition (GsMTx-4, SKF96365) was as efficient in abolishing chemotaxis as inhibition of signaling events downstream of the FGFR-1: PLC with 50 nM U73122 and PI3K with 50 nM Wortmannin. \* $p < 0.05$  (Student's  $t$  test)

enzymes blocked chemotaxis of hTRPC1-HA cells so that they moved randomly like siTRPC1 cells. This is manifested by values of the  $x$ -translocation of both cell types around zero. Noteworthy, only blocking of PLC resulted in a reduction of the mean velocity. Mean velocities of hTRPC1-HA- and of siTRPC1 cells were decreased by more than 50% to  $0.25 \pm 0.02$  and to  $0.24 \pm 0.03$   $\mu\text{m}/\text{min}$ , respectively. These results demonstrate that knockdown of TRPC1 channels or inhibition of lipid signaling abolished both directed migration toward the chemoattractant. However, only PLC inhibition impacted on velocity and directionality.

ERK1/2 (p44/42 MAPK) phosphorylation equals in hTRPC1-HA and siTRPC1 cells after FGF-2 stimulation

FGF-2 stimulation initiates various signaling events—an important one being the activation of ERK1/2 MAP kinases. Thus, we investigated the FGF-2 induced signaling further and compared ERK1/2 (p44/42 MAPK) phosphorylation in the two opposing cell lines hTRPC1-HA and siTRPC1. Figure 3a shows a Western Blot comparing ERK1/2 phosphorylation under control conditions ( $-$ FGF-2  $\pm$  the FGFR-1 inhibitor SU5402) and after 5 min stimulation with FGF-2 (10 ng/ml). Figure 3b provides a summary of these experiments. Under basal conditions ( $-$ FGF-2), we detected higher ERK1/2 phosphorylation in hTRPC1-HA cells than in siTRPC1 cells. Importantly, following FGF-2 stimulation, ERK1/2 phosphorylation in siTRPC1 increased to the same level as in hTRPC1-HA. Thus, the inability of siTRPC1 cells to chemotax along FGF-2 gradients cannot be ascribed to a

defect or absence of the FGF-2 receptor. Incubation with the FGFR-1 inhibitor SU5402 together with FGF-2 attenuated ERK1/2 phosphorylation.

FGF-2 stimulates a TRPC1-dependent  $\text{Ca}^{2+}$  influx

We next investigated the impact of FGF-2 stimulation on the cytosolic  $\text{Ca}^{2+}$  concentration (Fig. 4a). We found that serum-starved hTRPC1-HA cells had a mean  $[\text{Ca}^{2+}]_i$  of  $111 \pm 6$  nM. Serum-starved cells treated for 3 h with FGF-2 (10 ng/ml) had a significantly increased  $[\text{Ca}^{2+}]_i$  of  $151 \pm 6$  nM ( $n \geq 63$ ).  $[\text{Ca}^{2+}]_i$  of siTRPC1 cells was already higher ( $162 \pm 13$  nM) under control conditions. However,  $[\text{Ca}^{2+}]_i$  of siTRPC1 cells did not change following FGF-2 stimulation ( $164 \pm 13$  nM) ( $n \geq 45$ ). Noteworthy, we could not detect compensatory upregulation of other TRPC channels such as TRPC3 in

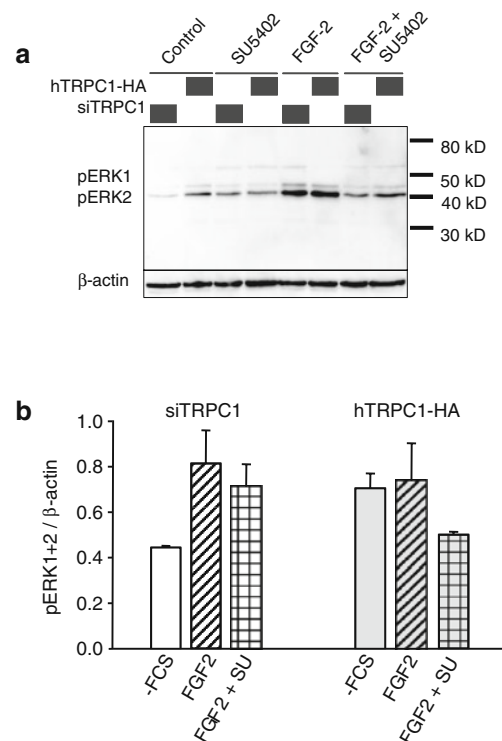


**Fig. 3** Western blot analysis demonstrating identical FGF-2 induced phosphorylation of ERK1/2 (p44/42 MAPK)—a major signaling event in the FGF-2 signaling cascade—in siTRPC1 and hTRPC1 cells. **a** A basal level of ERK1/2 phosphorylation was present in cell lysates from untreated ( $-$ FGF) MDCK-F cells. Also, after application of the FGF-R blocker SU5402 alone minor ERK1/2 phosphorylation could be detected. Phosphorylation of ERK1/2 increased in both cell lines to the same level in response to 5 min incubation with FGF-2 (10 ng/ml) indicating that FGF-receptor signaling is not affected by TRPC1 knockdown. Consequently, the FGF-2 dependent increase in ERK1/2 phosphorylation was prevented by co-application of SU5402. Staining of  $\beta$ -actin displays equal protein loading (lower panel). **b** Summary of four experiments. Here, we pooled the densitometric data for pERK1 and pERK2 and normalized them to the respective  $\beta$ -actin values

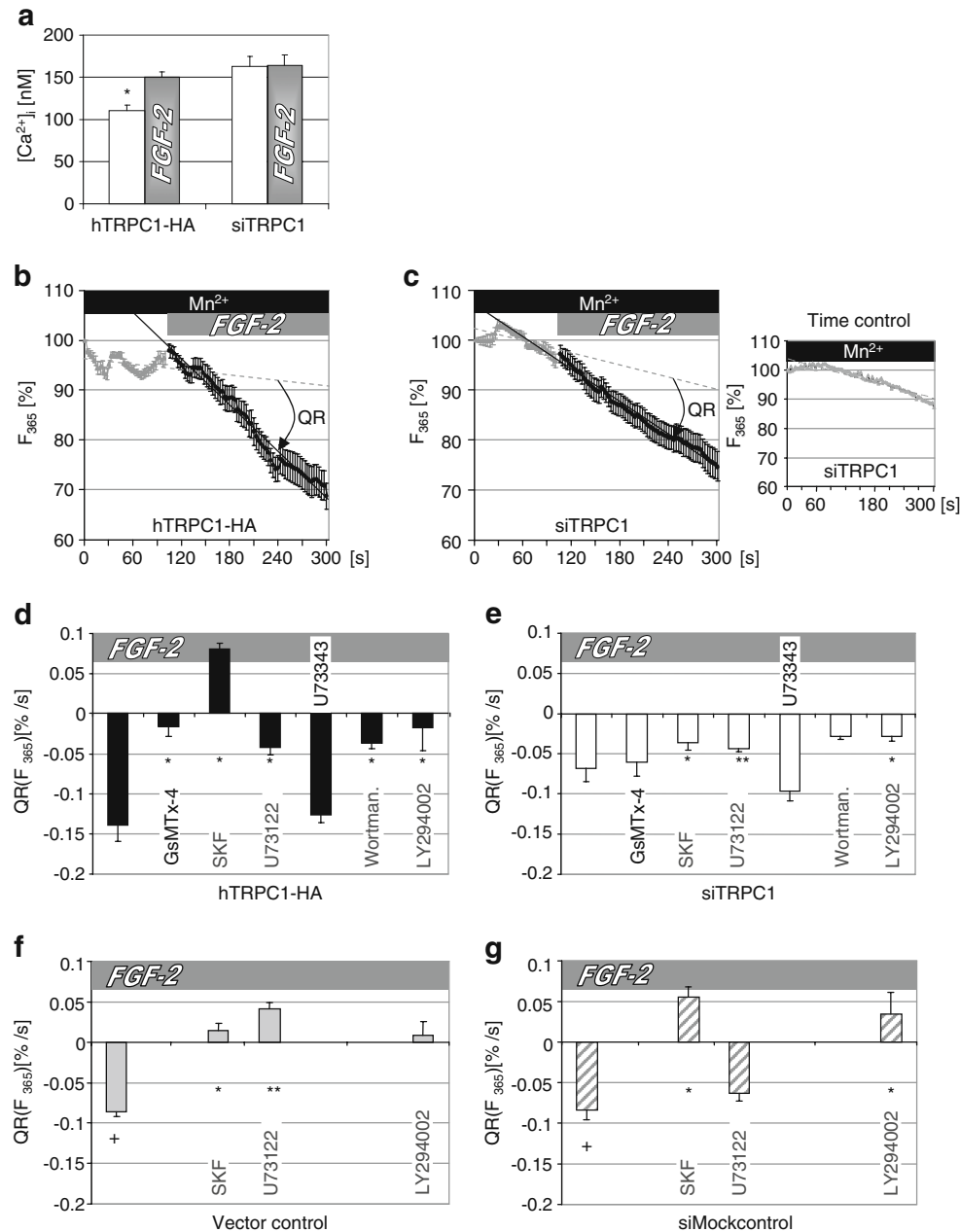


**Fig. 4** FGF-2 stimulates different  $\text{Ca}^{2+}$  responses in siTRPC1 cells compared to hTRPC1-HA overexpressing and respective controls (siMock and vector control cells). **a** Following a 3-h-long incubation with 10 ng/ml FGF-2  $[\text{Ca}^{2+}]_i$  of serum-starved hTRPC1-HA cells increased, whereas  $[\text{Ca}^{2+}]_i$  of siTRPC1 did not change. **b** Serum-starved cells were exposed to 50  $\mu\text{M}$   $\text{Mn}^{2+}$  to monitor the acute  $\text{Ca}^{2+}$  influx in response to 10 ng/ml FGF-2 by  $\text{Mn}^{2+}$  quenching of fura-2 fluorescence intensity  $F_{365}$ . The change in quenching rate QR ( $F_{365}$ ) before (dashed gray line) and after FGF-2 stimulation (black line) is taken as an indirect measure of  $\text{Ca}^{2+}$  influx. In hTRPC1-HA overexpressing cells, QR ( $F_{365}$ ) increased after application of 10 ng/ml FGF-2. **c** QR ( $F_{365}$ ) was only moderately changed by FGF-2 in siTRPC1 cells. Time control:  $\text{Mn}^{2+}$  quenching of a representative siTRPC1 cell without FGF-2 stimulation. **d** Summary of the  $\text{Mn}^{2+}$  quenching experiments. The FGF-2-dependent change in QR ( $F_{365}$ ) in

hTRPC1-HA cells was significantly attenuated by  $\text{Ca}^{2+}$  channel blockers (10  $\mu\text{M}$  GsMTx-4 and 25  $\mu\text{M}$  SKF96365) and inhibitors of phospholipid signaling (50 nM U73122, 50 nM Wortmannin, and LY294002), whereas the inactive analogue (U73343) had no effect. **e** In contrast, in siTRPC1 cells the FGF-2 induced  $\text{Ca}^{2+}$  entry, i.e., the change in QR ( $F_{365}$ ) was hardly affected by the same drugs. **f** In cells expressing the empty vector, a medium  $\text{Ca}^{2+}$  entry was observed that could be blocked by SKF, U73122, and LY204002. **g** The FGF-2 response of siMock cells was similar—the QR ( $F_{365}$ ) was between overexpressing and knockdown cells. SKF and LY 294002 reduced the response, but U73122 had nearly no effect on siMock cells. +, \* $p < 0.05$  (Student's *t* test); + indicates statistical difference between FGF-2 induced  $\text{Mn}^{2+}$  quench rates in hTRPC1-HA (**d**) or siTRPC1 cells (**e**) and the respective vector control cells (**f** and **g**, respectively)

these cells (see Fig. S1). TRPC3 expression is identical in all four cell lines tested in this study.

These findings prompted us to assess whether FGF-2 can also act acutely and elicit an instantaneous  $\text{Ca}^{2+}$  influx in the two opposing cell lines and controls. We monitored the  $\text{Ca}^{2+}$  influx by employing the fluorescence based  $\text{Mn}^{2+}$  quenching assay. Heavy metals such as  $\text{Mn}^{2+}$  can bind  $\text{Ca}^{2+}$  sensitive dyes such as fura-2 with higher affinity than  $\text{Ca}^{2+}$  resulting in fluorescence quenching effects. We performed paired experiments and determined the increase in quenching rate (QR ( $F_{365}$ )) following the application of FGF-2 (10 ng/ml). In hTRPC1-HA expressing cells, this increase amounts to QR ( $F_{365}$ ) =  $-0.139 \pm 0.020\%/s$  ( $n=52$ ), indicating an instantaneous  $\text{Ca}^{2+}$  influx upon FGF-2 stimulation (Fig. 4b). In contrast, FGF-2 elicited a greatly reduced response in siTRPC1 cells ( $-50\%$  as compared to hTRPC1-HA cells) (Fig. 4c). The mean quenching rate changed only by QR ( $F_{365}$ ) =  $-0.068 \pm 0.017\%/s$  ( $n=46$ ). The differential  $\text{Mn}^{2+}$  quench rates of MDCK-F cells with different expression levels of TRPC1 are consistent with the notion that TRPC1 channels constitute major  $\text{Ca}^{2+}$  entry channels activated upon FGF-2 stimulation. This was further promoted by the measurements of FGF-2 induced  $\text{Ca}^{2+}$  entry in the respective controls. Both the vector control and siMock control exhibited intermediate quenching rates lying between the values of hTRPC1-HA cells and siTRPC1 cells (Fig. 4f and g). The mean quenching rate of vector control cells changed by QR ( $F_{365}$ ) =  $-0.086 \pm 0.006\%/s$  ( $n=99$ ). The change in siMock cells was QR ( $F_{365}$ ) =  $-0.090 \pm 0.012\%/s$  ( $n=93$ ).  $\text{Mn}^{2+}$  quenching rates in both control cell lines were significantly different from hTRPC1-HA and siTRPC1 cells, respectively.

To provide further support for the interpretation that TRPC1 channels are responsive for the FGF-2 induced  $\text{Ca}^{2+}$  entry, we inhibited the  $\text{Ca}^{2+}$  influx with two different blockers (10  $\mu\text{M}$  GsMTx-4 and 25  $\mu\text{M}$  SKF96365) and monitored the changes in the rate of  $\text{Mn}^{2+}$  quenching (summary of  $\text{Mn}^{2+}$  quenching experiments in Fig. 4d–g). Both blockers prevented the FGF-2 induced change in the fluorescence quenching rate in hTRPC1-HA expressing cells. The mean quenching rate changed only by QR ( $F_{365}$ ) =  $-0.017 \pm 0.011\%/s$  ( $n=39$ ) in the presence of GsMTx-4 and reached a positive value of QR ( $F_{365}$ ) =  $0.081 \pm 0.008\%/s$  due ( $n=86$ ) following application of SKF96365. The latter result indicates that SKF96365 not only blocked FGF-2 induced  $\text{Ca}^{2+}$  influx but also basal  $\text{Ca}^{2+}$  influx. In contrast, siTRPC1 cells were insensitive to GsMTx-4 and only slightly sensitive to SKF96365. The mean quenching rate remained unchanged at QR ( $F_{365}$ ) =  $-0.060 \pm 0.018\%/s$  ( $n=28$ ) in presence of GsMTx-4. Application of FGF-2 together with SKF96365 only led to a small increase in  $\text{Mn}^{2+}$  quenching by QR ( $F_{365}$ ) =  $-0.036 \pm 0.010\%/s$  ( $n=57$ ) (Fig. 4e). SKF96365 also reduced the responses of vector and

siMock control cells to QR ( $F_{365}$ ) =  $0.015 \pm 0.009\%/s$  ( $n=73$ ) and QR ( $F_{365}$ ) =  $0.055 \pm 0.013\%/s$  ( $n=59$ ), respectively.

To get insights into the underlying activation mechanism of TRP channels we analyzed the impact of phospholipid signaling on the FGF-2 triggered  $\text{Ca}^{2+}$  influx (Fig. 4d–g). First, we applied an inhibitor of PLC U73122 (50 nM). PLC inhibition caused a marked reduction but not a full blockade of  $\text{Mn}^{2+}$  quenching in hTRPC1-HA cells. It decreased from QR ( $F_{365}$ ) =  $-0.139 \pm 0.020$  to  $-0.042 \pm 0.009\%/s$  ( $n=38$ ). In contrast,  $\text{Mn}^{2+}$  quenching was reduced to a much lesser extent by PLC blockade in siTRPC1 cells. It was lowered only from QR ( $F_{365}$ ) =  $-0.068 \pm 0.017$  to  $-0.043 \pm 0.004\%/s$  ( $n=71$ ). When we applied the inactive analogue U73343 together with FGF-2 we could observe almost the same change in QR as with FGF-2 alone—in the hTRPC1-HA cells we observed an increase by QR ( $F_{365}$ ) =  $-0.126 \pm 0.010\%/s$  ( $n=90$ ) and in siTRPC1 QR ( $F_{365}$ ) =  $-0.097 \pm 0.013\%/s$  ( $n=29$ ). In vector control cells, U73122 led to a change in QR ( $F_{365}$ ) =  $0.042 \pm 0.007\%/s$  ( $n=66$ ) indicating complete blockade of  $\text{Ca}^{2+}$  entry (Fig. 4f).  $\text{Ca}^{2+}$  entry into siMock could not be blocked by U73122 - QR ( $F_{365}$ ) =  $-0.063 \pm 0.009\%/s$  ( $n=109$ ) (Fig. 4g).

Next, we interfered with PI3K function by application of 50 nM Wortmannin or 10  $\mu\text{M}$  LY294002. hTRPC1-HA cells responded strongly and the FGF-2 induced quenching was reduced to a large extent by simultaneous application of FGF-2 and the different drugs (Wortmannin: QR ( $F_{365}$ ) =  $-0.037 \pm 0.007\%/s$ ;  $n=78$  and LY294002: QR ( $F_{365}$ ) =  $-0.018 \pm 0.028\%/s$ ;  $n=31$ ). In contrast, in siTRPC1 cells FGF-2 induced quenching was decreased to a much lesser extent (Wortmannin: QR ( $F_{365}$ ) =  $-0.028 \pm 0.004\%/s$ ;  $n=53$  and LY294002: QR ( $F_{365}$ ) =  $-0.028 \pm 0.006\%/s$ ;  $n=44$ ). In controls, application of LY294002 could prevent the FGF-2 induced  $\text{Ca}^{2+}$  influx as shown by changed quenching rates of QR ( $F_{365}$ ) =  $0.008 \pm 0.017\%/s$  ( $n=65$ ) for the vector control cells and QR ( $F_{365}$ ) =  $0.034 \pm 0.027\%/s$  ( $n=35$ ) for the siMock cells.

Taken together, these experiments show a consistent difference between TRPC1-HA overexpressing and siTRPC1 knockdown cells. FGF-2 induced  $\text{Mn}^{2+}$  quenching rates were much higher in hTRPC1-HA than in siTRPC1 cells and TRP channel blockers as well as PLC/PI3K blockers had almost no effect on siTRPC1 cells. These findings are consistent with the notion that FGF-2 leads to an activation of TRPC1 channels via lipid signaling.

#### TRPC1 and the FGFR-1 partially colocalize

Immunohistochemistry was performed to visualize the distribution of FGFR-1 and TRPC1 and to investigate the level of colocalization. To ensure specific labeling we performed adequate controls (see the Methods section). We employed antibodies against FGFR-1 and against HA to



stain the overexpressed hTRPC1-HA protein. Both membrane proteins were equally distributed throughout the entire cell (Fig. 5a). Epifluorescence images of TRPC1 and FGFR-1 signals were superimposed and the distances of pixels with highest fluorescence intensity were determined by line scans as shown in Fig. 5c. Dual-color signals whose optical centers that were less than 130 nm (corresponding to 1.0 pixel) apart from each other were classified as colocalizing signals. We counted single FGFR-1 signals or those FGFR-1 signals that were colocalizing with hTRPC1-HA signals in 5,000-pixel<sup>2</sup>-sized areas in 30 different cells ( $N=3$ ) and found 15.7% of all FGFR-1 spots colocalizing with hTRPC1-HA.

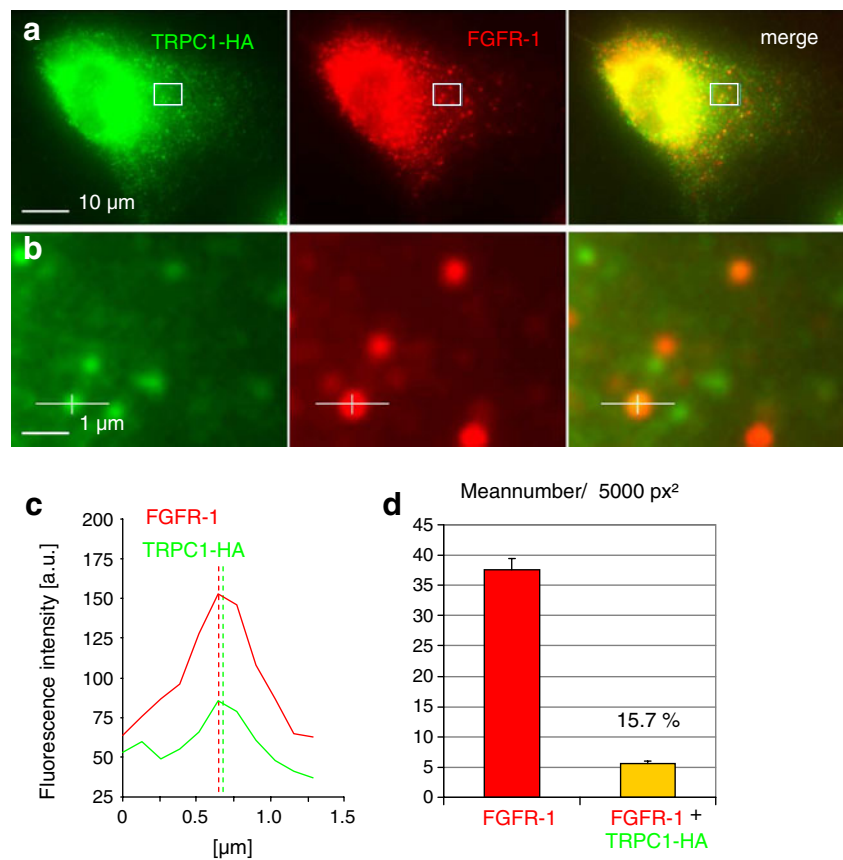
## Discussion

Path finding or movement in external chemical gradients is a basic physiologic mechanism for development, tissue homeostasis or also for the formation of tumor metastases. FGF-2 acts as mitogen in many cell types and is involved in growth of tumors from different origin [15, 22]. It can induce loss of epithelial properties in MDCK cells that heterologously express FGFR-1 [30]. Moreover, FGF-2 can directly stimulate migration of transformed MDCK cells

[18].  $\text{Ca}^{2+}$  has been identified as a key signaling molecule in directional sensing and migration [8, 16, 21, 35, 44, 45] but the connection between growth factor signaling and  $\text{Ca}^{2+}$  entry during chemotaxis still needs to be unravelled. Our study indicates that TRPC1 channels mediate the acute FGF-2 triggered  $\text{Ca}^{2+}$  entry, which seems to be crucial for the steering of chemotaxing MDCK-F cells that share some properties of tumor cells.

As the specificity of TRP channel blockers has been questioned we specifically addressed TRPC1 function by decreasing (by siRNA) or increasing (by overexpression) TRPC1 expression in two opposing stable cell lines. These cells were compared to the respective vector/mock control cell lines, which represent cells with endogenous TRPC1 expression. We found the following significant differences: (1) the ability to sense and migrate along an external FGF-2 gradient was blunted due to specific knockdown of TRPC1 while FGF-2 receptor signaling was intact; (2) unlike TRPC1 expressing cells, the knockdown cells did not increase  $[\text{Ca}^{2+}]_i$  in response to FGF-2 stimulation; (3) acute FGF-2 triggered TRPC1 mediated  $\text{Ca}^{2+}$  influx was at least ~50% higher in TRPC1 overexpressing cells than in knockdown cells. FGF-2-induced  $\text{Ca}^{2+}$  entry rates were of intermediate size in the control cell lines. Thus, the present study shows that disturbed intracellular  $\text{Ca}^{2+}$  distribution in

**Fig. 5** TRPC1 channels and FGF receptors partially colocalize. Epifluorescence images of TRPC1-HA overexpressing cells were dually labeled to examine the degree of colocalization between the channel and the FGF-2 receptor as measured by line scans. **a** The anti-TRPC1-HA (left) staining is evenly distributed similar to anti-FGFR-1 (center). Merging the dual-colored images revealed the significant amount of overlap (right). Bar=10  $\mu\text{m}$ . **b** 10 $\times$  magnified views of the white rectangles in panel **a** show single spots of maximum fluorescence intensity that were subjected to line scans as shown in panel **c**. Bar 1  $\mu\text{m}$ . **c** Line scans detected colocalization of intensity maxima of FGFR-1 (red) with TRPC1-HA (green). **d** Mean number of single FGFR-1-maxima (red) and FGFR-1 signals that colocalize with hTRPC1-HA (yellow) counted in 5,000-pixel<sup>2</sup>-sized areas ( $n=30$ ;  $N=3$ ). \* $p<0.05$  (Student's *t* test)



siTRPC1 cells cannot be overcome by an external chemoattractant stimulus.  $\text{Ca}^{2+}$  conveys intrinsic polarity to migrating cells in form of a narrow  $\text{Ca}^{2+}$  gradient within the lamellipodium. Ablation of TRPC1 leads to the breakdown of this gradient and is associated with significantly lower intrinsic directionality of migration [13]. These zones with high  $[\text{Ca}^{2+}]_i$  in a low- $\text{Ca}^{2+}$  background at the front of migrating cells contribute to defining front–rear polarity [44]. Thus, we propose that TRPC1 is rather involved in “steering” of cells than being the “motor of migration” during chemotaxis.

In addition to silencing and blockade of TRPC1 channels, inhibition of lipid signaling upstream of TRPC1 channels also interferes with the ability of MDCK-F cells to chemotax along FGF-2 gradients. The role of phospholipid signaling for directional movement has long been discussed (for review, see Ref. [20]). However, the connection to TRP channels has never been shown. In detail, studies in *Dictyostelium*, mammalian neutrophils and fibroblasts have shown that PI3Ks are locally activated at the leading edge of chemotaxing cells [17, 39, 41]. This spatially restricted activity could locally activate TRPC1 channels and promote the establishment of the  $\text{Ca}^{2+}$  gradient within the lamellipodium. Consequently, blockade of PI3K would impair downstream signaling to TRPC1 channels at the front and inhibition of chemotaxis. This study indeed shows that alternatively to TRPC1 knockdown also blockade of PI3K prevented directional movement toward FGF-2. Thus, both TRPC1 and PI3K seem to regulate directionality more than controlling cell motility itself. Consequently, activation of TRPC1 with FGF-2 did not increase the velocity and inhibition of TRPC1 directly or upstream via PI3K blockade only modestly decreased the velocity while abrogating chemotaxis. Noteworthy, inhibition of PLC interferes with both velocity and directionality, which is presumably because PLC is involved in multiple signaling events crucial for cell migration.

We further investigated the functional connection between FGF-2 stimulation and  $\text{Ca}^{2+}$  influx via TRPC1 channels in a time frame from a few minutes up to 3 h. We monitored  $[\text{Ca}^{2+}]_i$  after 3-h-long FGF-2 stimulation and the acute FGF-2 stimulated  $\text{Ca}^{2+}$  influx with the  $\text{Mn}^{2+}$  quenching technique. We detected an increase in the  $[\text{Ca}^{2+}]_i$  of hTRPC1-HA overexpressing cells in response to 3-h-long FGF-2 stimulation. These data correlate well with results gained in other cell types, in which FGF-2 activates SKF96365 sensitive currents mediated by TRPC1 [3]. Accordingly, knockdown of TRPC1 would interfere with these currents which could also explain why  $[\text{Ca}^{2+}]_i$  of siTRPC1 cells did not change in response to 3-h-long FGF-2 incubation. To date, we cannot state why  $[\text{Ca}^{2+}]_i$  was higher in serum-deprived siTRPC1 cells. We detected no compensatory upregulation of other TRPC channels. Thus,

Western blot analysis revealed that expression of TRPC3 channels is identical in all four cell lines used in this study. Similarly, RT-PCR experiments indicate that TRPC6 mRNA levels (normalized to GAPDH) are the same in siTRPC1 and the corresponding mock control cells. Presently, it is highly speculative to assume that a mutual regulation of TRPC1 and TRPC6 channels as it was recently described [37] underlies the elevation of  $[\text{Ca}^{2+}]_i$  in siTRPC1 cells. These authors provided evidence that TRPC6 channels are inhibited by TRPC1-mediated  $\text{Ca}^{2+}$  influx. Along these lines, TRPC1 knockdown would possibly cause a disinhibition of TRPC6 channels in siTRPC1 cells which could lead to an elevated  $[\text{Ca}^{2+}]_i$  and also account for the elevated basal  $\text{Mn}^{2+}$  quench rate in siTRPC1 cells. Noteworthy, the unresponsiveness of siTRPC1 cells to FGF-2 stimulation was not due to malfunction or downregulation of FGFR-1 in these cells. Due to the major signaling events caused by FGFR-1 activation ERK1/2 phosphorylation reached the same level in siTRPC1 and hTRPC1-HA cells.

Our results indicate that TRPC1 channels are a downstream target of FGF-2 induced phospholipid signaling because FGF-2 triggered  $\text{Ca}^{2+}$  influx could be impaired by blockade of PLC (U73122) or PI3K (wortmannin and LY294002). It is well established that TRPC channels are activated by PLC after activation by receptor tyrosine kinases or by G-protein coupled receptors [40]. PLC could possibly influence TRPC1 via DAG and  $\text{IP}_3$ . Although TRPC1 channels themselves are not stimulated by DAG their heteromultimerization with TRPC3 channels might convey indirect DAG sensitivity [9, 25, 26]. In fact, we confirmed by Western blot analysis that TRPC3 channels were expressed in MDCK-F cells.

PI3K producing primarily  $\text{PIP}_3$  from  $\text{PIP}_2$ , is blocked by 50 nM wortmannin or 10  $\mu\text{M}$  LY294002. In a recent study, receptor mediated activation of native TRPC1 channels in vascular myocytes was prevented by application of wortmannin or the PLC blocker U73122 [33]. We also see a blocking effect of these blockers on FGF-2 induced  $\text{Ca}^{2+}$  entry whereas the inactive analogue of U73122 (U73343) was ineffective. This suggests that PLC and PI3K are upstream in the signaling cascade that activates TRPC1 channels. There are reports showing effects of U73122 other than blocking PLC. Thus, it can apparently impair  $\text{Ca}^{2+}$  release from intracellular  $\text{Ca}^{2+}$  stores by blocking  $\text{Ca}^{2+}$  pumps [28]. However,  $\text{Ca}^{2+}$  pump inhibition cannot account for the reduction of the  $\text{Mn}^{2+}$  quench observed in our experiments.

Alternatively, the interplay between TRPC1 and PI3K in MDCK-F cells might resemble the positive feedback loop observed in macrophages. Here, the components  $\text{Ca}^{2+}$  entry, PI3K and F-actin dynamics maintain the organization of the active leading edge whereby the localized  $\text{Ca}^{2+}$  entry is the key for the specific localization at the front [12].

A third putative mechanism according for FGF-2 dependent activation of TRPC1 channels could be a direct interaction with activated FGFR-1. This possibility has to be taken into account since TRPC1 channels and FGFR-1 are in close spatial proximity within the plasma membrane as indicated by immunofluorescence colocalization studies that revealed a high overlap frequency of TRPC1 and FGFR-1. A similar colocalization of TRPC1 and FGFR-1 was observed in the developing brain [14].

Combining our findings of the chemotaxis experiments and  $\text{Ca}^{2+}$  measurements, we conclude that FGF-2 stimulation activates a  $\text{Ca}^{2+}$  influx via PLC and PI3K dependent activation of TRPC1 channels. This  $\text{Ca}^{2+}$  influx is crucial for chemotaxis toward FGF-2. Accordingly, silencing of TRPC1 led to FGF-2 insensitivity. Future studies will reveal whether this mechanism can be transferred from the MDCK-F cell model to preclinical tumor models in an effort to impair tumor metastasis.

**Acknowledgement** This work was supported by grants from the Rolf-Dierichs-Stiftung (Medical Faculty, University Münster) (grant number: 193423) and from the Boehringer Ingelheim Fonds to A.F.. A.S. was supported by the IZKF Münster (grant number: Schw 2/030/08) and by the Deutsche Forschungsgemeinschaft (grant number: Schw 407/9-3).

**Ethical approval** All experiments were performed in accordance with the ethical standards required by *Pflügers Archiv–European Journal of Physiology*.

**Conflicts of interest** The authors declare that they have no conflict of interest.

## References

- Abramowitz J, Birnbaumer L (2009) Physiology and pathophysiology of canonical transient receptor potential channels. *FASEB J* 23:297–328
- Ahmed GU, Mehta D, Vogel S, Holinstat M, Paria BC, Tirupathi C, Malik AB (2004) Protein kinase C $\alpha$  phosphorylates the TRPC1 channel and regulates store-operated  $\text{Ca}^{2+}$  entry in endothelial cells. *J Biol Chem* 279:20941–20949
- Antonietti S, Lovisolo D, Fiorio Pla A, Munaron L (2002) Expression and functional role of bTRPC1 channels in native endothelial cells. *FEBS Lett* 510:189–195
- Ashish PMS, Perryman PB, Yang L, Yin HL, Krueger JK (2007) Global structure changes associated with  $\text{Ca}^{2+}$  activation of full-length human plasma gelsolin. *J Biol Chem* 282:25884–25892
- Bandyopadhyay BC, Swaim WD, Liu X, Redman RS, Patterson RL, Ambudkar IS (2005) Apical localization of a functional TRPC3/TRPC6- $\text{Ca}^{2+}$ -signaling complex in polarized epithelial cells. Role in apical  $\text{Ca}^{2+}$  influx. *J Biol Chem* 280:12908–12916
- Bowman CL, Gottlieb PA, Suchyna TM, Murphy YK, Sachs F (2007) Mechanosensitive ion channels and the peptide inhibitor GsMTx-4: history, properties, mechanisms and pharmacology. *Toxicol* 49:249–270
- Brazer SC, Singh BB, Liu X, Swaim W, Ambudkar IS (2003) Caveolin-1 contributes to assembly of store-operated  $\text{Ca}^{2+}$  influx channels by regulating plasma membrane localization of TRPC1. *J Biol Chem* 278:27208–27215
- Brundage RA, Fogarty KE, Tuft RA, Fay FS (1991) Calcium gradients underlying polarization and chemotaxis of eosinophils. *Science* 254:703–706
- Chen J, Crossland RF, Noorani MMZ, Marrelli SP (2009) Inhibition of TRPC1/TRPC3 by PKG contributes to NO-mediated vasorelaxation. *Am J Physiol Heart Circ Physiol* 297:H417–H424
- Doyle AD, Lee J (2005) Cyclic changes in keratocyte speed and traction stress arise from  $\text{Ca}^{2+}$ -dependent regulation of cell adhesiveness. *J Cell Sci* 118:369–379
- Draval V, Dieterich P, Stock C, Schwab A (2005) The role of  $\text{Ca}^{2+}$  transport across the plasma membrane for cell migration. *Cell Physiol Biochem* 16:119–126
- Evans JH, Falke JJ (2007)  $\text{Ca}^{2+}$  influx is an essential component of the positive-feedback loop that maintains leading-edge structure and activity in macrophages. *Proc Natl Acad Sci USA* 104:16176–16181
- Fabian A, Fortmann T, Dieterich P, Riethmüller C, Schön P, Mally S, Nilius B, Schwab A (2008) TRPC1 channels regulate directionality of migrating cells. *Pflugers Arch* 457:475–484
- Fiorio Pla A, Maric D, Brazer SC, Giacobini P, Liu X, Chang YH, Ambudkar IS, Barker JL (2005) Canonical transient receptor potential 1 plays a role in basic fibroblast growth factor (bFGF)/FGF receptor-1-induced  $\text{Ca}^{2+}$  entry and embryonic rat neural stem cell proliferation. *J Neurosci* 25:2687–2701
- Guerrin M, Scotet E, Malecaze F, Houssaint E, Plouet J (1997) Overexpression of vascular endothelial growth factor induces cell transformation in cooperation with fibroblast growth factor 2. *Oncogene* 14:463–471
- Hahn K, DeBiasio R, Taylor DL (1992) Patterns of elevated free calcium and calmodulin activation in living cells. *Nature* 359:736–738
- Haugh JM, Codazzi F, Teruel M, Meyer T (2000) Spatial sensing in fibroblasts mediated by 3' phosphoinositides. *J Cell Biol* 151:1269–1280
- Hofmann T, Obukhov AG, Schaefer M, Harteneck C, Gudermann T, Schultz G (1999) Direct activation of human TRPC6 and TRPC3 channels by diacylglycerol. *Nature* 397:259–263
- Kessler W, Budde T, Gekle M, Fabian A, Schwab A (2008) Activation of cell migration with fibroblast growth factor-2 requires calcium-sensitive potassium channels. *Pflugers Arch* 456:813–823
- Kölsch V, Charest PG, Firtel RA (2008) The regulation of cell motility and chemotaxis by phospholipid signaling. *J Cell Sci* 121:551–559
- Komuro H, Rakic P (1996) Intracellular  $\text{Ca}^{2+}$  fluctuations modulate the rate of neuronal migration. *Neuron* 17:275–285
- Kwabi-Addo B, Ozen M, Ittmann M (2004) The role of fibroblast growth factors and their receptors in prostate cancer. *Endocr Relat Cancer* 11:709–724
- Lee J, Ishihara A, Oxford G, Johnson B, Jacobson K (1999) Regulation of cell movement is mediated by stretch-activated calcium channels. *Nature* 400:382–386
- Lemonnier L, Trebak M, Putney JW Jr (2008) Complex regulation of the TRPC3, 6 and 7 channel subfamily by diacylglycerol and phosphatidylinositol-4, 5-bisphosphate. *Cell Calcium* 43:506–514
- Lintschinger B, Balzer-Geldsetzer M, Baskaran T, Graier WF, Romanin C, Zhu MX, Groschner K (2000) Coassembly of Trp1 and Trp3 proteins generates diacylglycerol- and  $\text{Ca}^{2+}$ -sensitive cation channels. *J Biol Chem* 275:27799–27805
- Liu X, Bandyopadhyay BC, Singh BB, Groschner K, Ambudkar IS (2005) Molecular analysis of a store-operated and 2-acetyl-sn-glycerol-sensitive non-selective cation channel. Heteromeric assembly of TRPC1-TRPC3. *J Biol Chem* 280:21600–21606

27. Louis M, Zanou N, Van Schoor M, Gailly P (2008) TRPC1 regulates skeletal myoblast migration and differentiation. *J Cell Sci* 121:3951–3959
28. MacMillan D, McCarron JG (2010) The phospholipase C inhibitor U-73122 inhibits  $\text{Ca}^{2+}$  release from the intracellular sarcoplasmic reticulum  $\text{Ca}^{2+}$  store by inhibiting  $\text{Ca}^{2+}$  pumps in smooth muscle. *Br J Pharmacol* 160:1295–1301
29. Merritt JE, Jacob R, Hallam TJ (1989) Use of manganese to discriminate between calcium influx and mobilization from internal stores in stimulated human neutrophils. *J Biol Chem* 264:1522–1527
30. Migdal M, Soker S, Yarden Y, Neufeld G (1995) Activation of a transfected FGFR-1 receptor in Madin-Darby epithelial cells results in a reversible loss of epithelial properties. *J Cell Physiol* 162:266–276
31. Munaron L, Fiorio Pla A (2000) Calcium influx induced by activation of tyrosine kinase receptors in cultured bovine aortic endothelial cells. *J Cell Physiol* 185:454–456
32. Oberleithner H, Westphale HJ, Gassner B (1991) Alkaline stress transforms Madin–Darby canine kidney cells. *Pflugers Arch* 419:418–420
33. Saleh SN, Albert AP, Large WA (2009) Activation of native TRPC1/C5/C6 channels by endothelin-1 is mediated by both PIP(3) and PIP(2) in rabbit coronary artery myocytes. *J Physiol* 587:5361–5375
34. Saleh SN, Albert AP, Peppiatt-Wildman CM, Large WA (2008) Diverse properties of store-operated TRPC channels activated by protein kinase C in vascular myocytes. *J Physiol* 586:2463–2476
35. Schwab A, Finsterwalder F, Kersting U, Danker T, Oberleithner H (1997) Intracellular  $\text{Ca}^{2+}$  distribution in migrating transformed epithelial cells. *Pflugers Arch* 434:70–76
36. Schwab A, Nechyporuk-Zloy V, Fabian A, Stock C (2007) Cells move when ions and water flow. *Pflugers Arch* 453:421–432
37. Shi J, Ju M, Saleh SN, Albert AP, Large WA (2010) TRPC6 channels stimulated by angiotensin II are inhibited by TRPC1/C5 channel activity through a  $\text{Ca}^{2+}$ - and PKC-dependent mechanism in native vascular myocytes. *J Physiol* 588:3671–3682
38. Shim S, Goh EL, Ge S, Sailor K, Yuan JP, Roderick HL, Bootman MD, Worley PF, Song H, Ming GL (2005) XTRPC1-dependent chemotropic guidance of neuronal growth cones. *Nat Neurosci* 8:730–735
39. Takeda K, Sasaki AT, Ha H, Seung HA, Firtel RA (2007) Role of phosphatidylinositol 3-kinases in chemotaxis in *Dictyostelium*. *J Biol Chem* 282:11874–11884
40. Trebak M, Lemonnier L, Smyth JT, Vazquez G, Putney Jr JW (2007) Phospholipase C-coupled receptors and activation of TRPC channels. *Handb Exp Pharmacol*:593–614
41. Wang F, Herzmark P, Weiner OD, Srinivasan S, Servant G, Boume HR (2002) Lipid products of PI(3)Ks maintain persistent cell polarity and directed motility in neutrophils. *Nat Cell Biol* 4:513–518
42. Wang GX, Poo MM (2005) Requirement of TRPC channels in netrin-1-induced chemotropic turning of nerve growth cones. *Nature* 434:898–904
43. Waning J, Vriens J, Owsianik G, Stuwe L, Mally S, Fabian A, Fripiat C, Nilius B, Schwab A (2007) A novel function of capsaicin-sensitive TRPV1 channels: involvement in cell migration. *Cell Calcium* 42:17–25
44. Wei C, Wang X, Chen M, Ouyang K, Song LS, Cheng H (2009) Calcium flickers steer cell migration. *Nature* 457:901–905
45. Xu HT, Yuan XB, Guan CB, Duan S, Wu CP, Feng L (2004) Calcium signaling in chemorepellant Slit2-dependent regulation of neuronal migration. *Proc Natl Acad Sci USA* 101:4296–4301
46. Yang S, Zhang JJ, Huang XY (2009) Orail and STIM1 are critical for breast tumor cell migration and metastasis. *Cancer Cell* 15:124–134